Characteristics of Striplines With Inhomogeneous Cylindrical Substrate

Jean-Fu Kiang, *Member, IEEE*, Chung-Rung Lee, and Chun Hsiung Chen, *Fellow, IEEE*

***Abstract*—A mode-matching technique combined with Galerkin's method is proposed in this paper to analyze the characteristics of striplines embedded in an inhomogeneous cylindrical medium. The potential in each layer is expressed in terms of eigenmodes obtained numerically. Coupling between two sets of eigenmodes in contiguous layers is described by defining potential ratio coefficient matrices. An integral equation is derived based on these eigenmodes with charge on the stripline as unknown. The method of moments is then applied to solve this integral equation. Various parameters are analyzed for their effects on transmission characteristics.**

***Index Terms*—Cylindrical striplines, Galerkin's method, inhomogeneous, integral equation, layered medium, mode matching, transmission characteristics.**

I. Introduction

CYLINDRICAL striplines can be used in designing balun, slotted line, coaxial-to-planar line transition adapters, impedance transformers, filters, feed networks of cylindrical antennas, etc. Recent advances in integrated circuit (IC) technology also make the multiconductor transmission line an important component in high-speed digital ICs. However, the design of passive circuits on curved surfaces or in an inhomogeneous medium is difficult with most numerical approaches [1], [2]. The problems of cylindrical or elliptical transmission lines have been analyzed by using various techniques including the conformal-mapping technique [3]–[5], iterative approach [6], variational approach [7], method of lines [1], [8], method of moments [9], [10], modified residue calculus technique [11], finite- and infinite-element methods [12], finite-difference time-domain method [13]–[15], etc.

For cylindrical microstrip lines and striplines in a less complicated layered medium, approximate closed-form solutions can be obtained [16], [17]. In [7], a variational technique in the spectral domain is developed to study arbitrary multiconductor and multidielectric cylindrical striplines. In [18], a cylindrical microstrip line in a half-open space is studied. In [13], impedance matching at the junction of a coaxial transmission line and a cylindrical microstrip line is achieved by adjusting the radius or the dielectric constant. In [15], three-dimensional (3-D) structures of cylindrical coplanar waveguide filters are studied by using the finite-difference time-domain method.

Conformal-mapping technique can only be used to calculate static parameters rather than frequency-dependent parameters of the microstrip. In [10], the dyadic Green's function is used to derive a full-wave analysis in the form of Fourier series, and the dispersion properties are determined by using Galerkin's method. In [19], the dielectric constant in each layer is assumed to be a function of the transversal direction in the Cartesian coordinates. This approach can be extended to study cylindrical microstrip lines on an inhomogeneous layered medium by using a conformal-mapping technique.

In this paper, an alternative approach is proposed by applying the mode-matching technique with Galerkin's method directly to the cylindrical problems. Each layer of the cylindrical substrate in all the above references, except [2] and [20], is considered as a homogeneous medium. In [2], the dielectric constant of the cylindrical microstrip lines is assumed as a function of radius. In [20], the dielectric constant in each layer of the wedge-supported cylindrical microstrip lines with an indented ground is a function of the azimuthal angle. In this paper, it is emphasized that the medium in each layer is inhomogeneous in the azimuthal direction, where local inhomogeneities near the stripline can be utilized to adjust the phase velocities of the guided-wave modes. A concise description of this study was presented in [21].

In Section II, a generalized Laplace equation in cylindrical coordinates is derived first, and is then solved by using the separation-of-variable technique and an eigenmode analysis. The eigenmodes thus obtained are used to expand the potential distribution in each inhomogeneous layer; an integral equation is then formulated by matching proper boundary conditions. Finally, Galerkin's method is applied to solve the integral equation for the charge distribution on the strip from which the transmission characteristics are derived.

II. Formulation

Fig. 1 shows the cross section of a uniform stripline embedded in an inhomogeneous cylindrically layered medium. The configuration is uniform in the z-direction, and the dielectric constant in each layer is a function of the azimuthal angle, i.e., $\epsilon = \epsilon(\phi)$. The electrostatic field can be derived from a potential distribution, and satisfies the Gauss law as

$$\overline{E}(\overline{r}) = -\nabla\Psi(\overline{r})$$
$$\nabla \cdot \overline{D}(\overline{r}) = \zeta(\overline{r}) \tag{1}$$

Manuscript received February 22, 2002; revised August 6, 2002. This work was supported by the National Science Council, Taiwan, R.O.C., under Contract NSC89-2213-E-002-181.

J.-F. Kiang and C. H. Chen are with the Department of Electrical Engineering and Graduate Institute of Communication Engineering, National Taiwan University, Taipei, Taiwan 106, R.O.C. (e-mail: jfkiang@cc.ee.ntu.edu.tw).

C.-R. Lee was with the Department of Electrical Engineering and Graduate Institute of Communication Engineering, National Taiwan University, Taipei, Taiwan 106, R.O.C. He is now with the Department of Wireless Communication Production, MediaTek Inc., Taiwan 300, R.O.C.

Digital Object Identifier 10.1109/TMTT.2003.810130

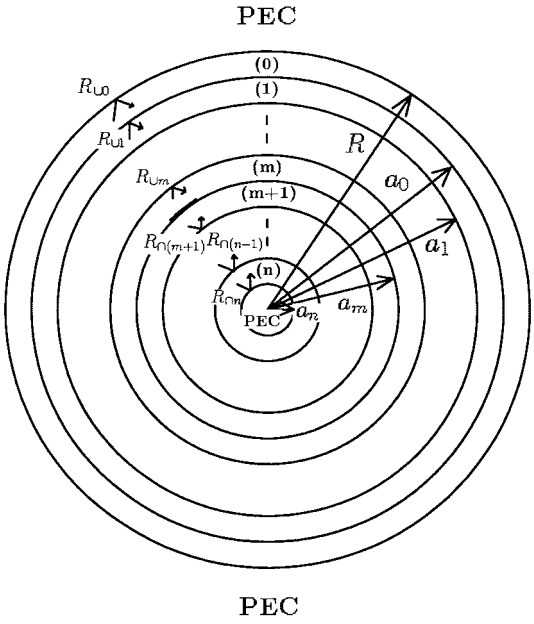

Fig. 1. Cross-sectional view of a stripline embedded in a cylindrical inhomogeneous medium.

where $\Psi(\overline{r})$ is the potential distribution, $\overline{E}(\overline{r})$ is the electrostatic field, $\overline{D}(\overline{r})$ is the electric flux density function, and $\zeta(\overline{r})$ is the charge distribution. The potential distribution can be shown to satisfy the Poisson's equation in the cylindrical coordinates as

$$\rho\frac{\partial}{\partial\rho}\left[\rho\frac{\partial}{\partial\rho}\Psi(\rho,\,\phi)\right]+\frac{1}{\epsilon(\phi)}\frac{\partial}{\partial\phi}\left[\epsilon(\phi)\frac{\partial}{\partial\phi}\Psi(\rho,\,\phi)\right]=-\rho^2\frac{\zeta(\rho,\phi)}{\epsilon(\phi)}. \quad (2)$$

In the absence of charge, the Poisson equation is reduced to the following generalized Laplace equation:

$$\rho\frac{\partial}{\partial\rho}\left[\rho\frac{\partial}{\partial\rho}\Psi(\rho,\,\phi)\right]+\frac{1}{\epsilon(\phi)}\frac{\partial}{\partial\phi}\left[\epsilon(\phi)\frac{\partial}{\partial\phi}\Psi(\rho,\,\phi)\right]=0. \quad (3)$$

Using the separation-of-variable technique, the potential distribution is first expressed as a product of functions of ρ and ϕ, respectively, as

$$\Psi(\rho,\,\phi)=\psi(\rho)\eta(\phi) \quad (4)$$

where $\psi(\rho)$ and $\eta(\phi)$ satisfy separate harmonic equations as

$$\rho\frac{\partial}{\partial\rho}\left[\rho\frac{\partial\psi(\rho)}{\partial\rho}\right]=k^2\psi(\rho)$$
$$\frac{1}{\epsilon(\phi)}\frac{\partial}{\partial\phi}\left[\epsilon(\phi)\frac{\partial\eta(\phi)}{\partial\phi}\right]=-k^2\eta(\phi) \quad (5)$$

with the separation constant k^2. When the dielectric constant is independent of ϕ, the solutions to (5) reduce to the following mode functions:

$$S_p(\phi)=\begin{cases}\cos(p\phi/2), & p=0,\,2,\,4,\,\ldots\\ \sin\left[(p+1)\phi/2\right], & p=1,\,3,\,5,\,\ldots\end{cases} \quad (6)$$

which satisfy the orthonormality properties that

$$\left\langle S_p(\phi),\,S_q(\phi)\right\rangle=\int_0^{2\pi}S_p(\phi)S_q(\phi)\,d\phi=\delta_{pq}. \quad (7)$$

Assume that the solutions to (5) in the presence of an inhomogeneous medium can be expressed as a superposition of the mode functions $\{S_p(\phi)\}$ as

$$\eta_n(\phi)=\sum_{p=0}^{N-1}b_{np}S_p(\phi) \quad (8)$$

where the expansion is truncated to the first N mode functions. Substituting (8) into (5), we have

$$\sum_{p=0}^{N-1}b_{np}\frac{\partial}{\partial\phi}\left[\epsilon(\phi)\frac{\partial}{\partial\phi}S_p(\phi)\right]=-k_n^2\sum_{p=0}^{N-1}b_{np}S_p(\phi)\epsilon(\phi). \quad (9)$$

Taking the inner product of each mode function $\{S_q(\phi)\}$ with (9), we obtain the following eigenmatrix equation:

$$\sum_{p=0}^{N-1}\left\langle S_q'(\phi)\epsilon(\phi)S_p'(\phi)\right\rangle b_{np}=k_n^2\sum_{p=0}^{N-1}\left\langle S_q(\phi)\epsilon(\phi)S_p(\phi)\right\rangle b_{np},\qquad 0\le q<N \quad (10)$$

where k_n^2 is the nth eigenvalue associated with the nth eigenvector $\overline{b}_n=[b_{n0},\,b_{n1},\,\ldots,\,b_{n(N-1)}]^t$. The coefficients $\{b_{np}\}$ are normalized to let the eigenfunctions $\{\eta_s(\phi)\}$ satisfy the orthonormality condition that $\langle\eta_r(\phi)\epsilon(\phi)\eta_s(\phi)\rangle=\delta_{rs}$ or $\overline{b}_r^{\,t}\cdot\overline{\overline{C}}\cdot\overline{b}_s=\delta_{rs}$ with the qpth element of $\overline{\overline{C}}$ being $\langle S_q(\phi)\epsilon(\phi)S_p(\phi)\rangle$.

The potential distribution in each layer can be expressed in terms of the eigenfunctions in that layer as

$$\Psi_0(\rho,\,\phi)=\overline{\eta}_0^{\,t}(\phi)\cdot\left[\overline{\overline{F}}_{0+}(\rho)\cdot\overline{a}_0+\overline{\overline{F}}_{0-}(\rho)\cdot\overline{b}_0\right]$$
$$\Psi_\ell(\rho,\,\phi)=\overline{\eta}_\ell^{\,t}(\phi)\cdot\left[\overline{\overline{F}}_{\ell+}(\rho)\cdot\overline{a}_\ell+\overline{\overline{F}}_{\ell-}(\rho)\cdot\overline{b}_\ell\right],\qquad 1\le\ell\le n \quad (11)$$

where $\overline{a}_0$, $\overline{b}_0$, $\overline{a}_\ell$, and $\overline{b}_\ell$ are vectors containing the expansion coefficients in each layer, $\overline{\eta}_\ell(\phi)=[\eta_0(\phi),\,\eta_1(\phi),\,\ldots,\,\eta_{N-1}(\phi)]^t$, $\overline{\overline{F}}_{0\pm}(\rho)$, and $\overline{\overline{F}}_{\ell\pm}(\rho)$ are diagonal matrices with $\overline{\overline{F}}_{\ell\pm}(\rho)=\text{diag.}\,[f_{\ell0\pm}(\rho),\,f_{\ell1\pm}(\rho),\,\ldots,\,f_{\ell(N-1)\pm}(\rho)]$, and

$$f_{0p+}(\rho)=\begin{cases}(\rho/R)^{-k_p}, & k_p\ne0\\ \ln(\rho/R), & k_p=0\end{cases}$$
$$f_{0p-}(\rho)=\begin{cases}(\rho/R)^{k_p}, & k_p\ne0\\ 1, & k_p=0\end{cases}$$
$$f_{\ell p+}(\rho)=\begin{cases}(\rho/a_\ell)^{-k_p}, & k_p\ne0\\ \ln(\rho/a_\ell), & k_p=0\end{cases}$$
$$f_{\ell p-}(\rho)=\begin{cases}(\rho/a_\ell)^{k_p}, & k_p\ne0\\ 1, & k_p=0\end{cases} \quad (12)$$

with $\ell\ne0$.

To facilitate the derivation, define potential ratio coefficient matrices $\overline{\overline{R}}_{\cap\ell}$ at $\rho = a_\ell$ and $\overline{\overline{R}}_{\cup\ell}$ at $\rho = a_{\ell-1}$ in layer (ℓ) such that

$$\begin{aligned}\overline{\overline{F}}_{\ell+}(a_\ell)\cdot\overline{a}_\ell &= \overline{\overline{R}}_{\cap\ell}\cdot\overline{\overline{F}}_{\ell-}(a_\ell)\cdot\overline{b}_\ell \\ \overline{\overline{F}}_{\ell-}(a_{\ell-1})\cdot\overline{b}_\ell &= \overline{\overline{R}}_{\cup\ell}\cdot\overline{\overline{F}}_{\ell+}(a_{\ell-1})\cdot\overline{a}_\ell. \end{aligned} \tag{13}$$

The potential in layer (ℓ) is thus expressed as

$$\begin{aligned}\Psi_0(\rho,\phi) &= \overline{\eta}_0^t(\phi)\cdot\left[\overline{\overline{F}}_{0+}(\rho)+\overline{\overline{F}}_{0-}(\rho)\cdot\overline{\overline{F}}_{0-}^{-1}(R)\cdot\overline{\overline{R}}_{\cup 0}\cdot\overline{\overline{F}}_{0+}(R)\right]\cdot\overline{a}_0 \\ \Psi_\ell(\rho,\phi) &= \overline{\eta}_\ell^t(\phi)\cdot\left[\overline{\overline{F}}_{\ell+}(\rho)+\overline{\overline{F}}_{\ell-}(\rho)\cdot\overline{\overline{F}}_{\ell-}^{-1}(a_{\ell-1})\cdot\overline{\overline{R}}_{\cup\ell}\cdot\overline{\overline{F}}_{\ell+}(a_{\ell-1})\right]\cdot\overline{a}_\ell, \qquad 1\le\ell\le m \\ \Psi_\ell(\rho,\phi) &= \overline{\eta}_\ell^t(\phi)\cdot\left[\overline{\overline{F}}_{\ell+}(\rho)\cdot\overline{\overline{F}}_{\ell+}^{-1}(a_\ell)\cdot\overline{\overline{R}}_{\cap\ell}\cdot\overline{\overline{F}}_{\ell-}(a_\ell)+\overline{\overline{F}}_{\ell-}(\rho)\right]\cdot\overline{b}_\ell, \qquad m+1\le\ell\le n. \end{aligned} \tag{14}$$

Assume that a perfect electric conductor is placed at $\rho = R$ as a reference, which implies $\Psi_0(R,\phi) = 0$. Thus, we have $\overline{\overline{R}}_{\cup 0} = -\overline{\overline{I}}$ with $\overline{\overline{I}}$ being an identity matrix. At $\rho = a_0$, impose the boundary conditions that the potential and normal electric flux density are continuous, i.e., $\Psi_0(a_0,\phi) = \Psi_1(a_0,\phi)$ and $\epsilon_0(\phi)\partial\Psi_0(a_0,\phi)/\partial\rho = \epsilon_1(\phi)\partial\Psi_1(a_0,\phi)/\partial\rho$. By applying these conditions to the potential distributions in (14), we have

$$\begin{aligned}&\left[\overline{\overline{F}}_{0+}(a_0)+\overline{\overline{F}}_{0-}(a_0)\cdot\overline{\overline{F}}_{0-}^{-1}(R)\cdot\overline{\overline{R}}_{\cup 0}\cdot\overline{\overline{F}}_{0+}(R)\right]\cdot\overline{a}_0 \\ &=\overline{\overline{H}}_{01}\cdot\left[\overline{\overline{F}}_{1+}(a_0)+\overline{\overline{F}}_{1-}(a_0)\cdot\overline{\overline{F}}_{1-}^{-1}(a_0)\cdot\overline{\overline{R}}_{\cup 1}\cdot\overline{\overline{F}}_{1+}(a_0)\right]\cdot\overline{a}_1 \\ &\left[\overline{\overline{F}}'_{0+}(a_0)+\overline{\overline{F}}'_{0-}(a_0)\cdot\overline{\overline{F}}_{0-}^{-1}(R)\cdot\overline{\overline{R}}_{\cup 0}\cdot\overline{\overline{F}}_{0+}(R)\right]\cdot\overline{a}_0 \\ &=\overline{\overline{H}}_{10}^t\cdot\left[\overline{\overline{F}}'_{1+}(a_0)+\overline{\overline{F}}'_{1-}(a_0)\cdot\overline{\overline{F}}_{1-}^{-1}(a_0)\cdot\overline{\overline{R}}_{\cup 1}\cdot\overline{\overline{F}}_{1+}(a_0)\right]\cdot\overline{a}_1 \end{aligned} \tag{15}$$

where $\overline{\overline{H}}_{ij} = \langle\epsilon_i(\phi)\overline{\eta}_i(\phi)\overline{\eta}_j^t(\phi)\rangle$. Eliminating $\overline{a}_0$ and $\overline{a}_1$, we have

$$\begin{aligned}&\left[\overline{\overline{F}}_{0+}(a_0)+\overline{\overline{F}}_{0-}(a_0)\cdot\tilde{\overline{\overline{R}}}_{\cup 0}\right]^{-1}\cdot\overline{\overline{H}}_{01}\cdot\left[\overline{\overline{F}}_{1+}(a_0)+\overline{\overline{F}}_{1-}(a_0)\cdot\tilde{\overline{\overline{R}}}_{\cup 1}\right] \\ &=\left[\overline{\overline{F}}'_{0+}(a_0)+\overline{\overline{F}}'_{0-}(a_0)\cdot\tilde{\overline{\overline{R}}}_{\cup 0}\right]^{-1}\cdot\overline{\overline{H}}_{10}^t\cdot\left[\overline{\overline{F}}'_{1+}(a_0)+\overline{\overline{F}}'_{1-}(a_0)\cdot\tilde{\overline{\overline{R}}}_{\cup 1}\right] \end{aligned} \tag{16}$$

where the normalized potential ratio coefficient matrices are defined as

$$\begin{aligned}\tilde{\overline{\overline{R}}}_{\cup\ell} &= \overline{\overline{F}}_{\ell-}^{-1}(a_{\ell-1})\cdot\overline{\overline{R}}_{\cup\ell}\cdot\overline{\overline{F}}_{\ell+}(a_{\ell-1}) \\ \tilde{\overline{\overline{R}}}_{\cup 0} &= \overline{\overline{F}}_{0-}^{-1}(R)\cdot\overline{\overline{R}}_{\cup 0}\cdot\overline{\overline{F}}_{0+}(R). \end{aligned} \tag{17}$$

The explicit form of $\overline{\overline{R}}_{\cup 1}$ can be derived from (16) as

$$\begin{aligned}&\overline{\overline{R}}_{\cup 1} \\ &=\overline{\overline{F}}_{1-}(a_0) \\ &\cdot\left\{\left[\overline{\overline{F}}_{0+}(a_0)+\overline{\overline{F}}_{0-}(a_0)\cdot\tilde{\overline{\overline{R}}}_{\cup 0}\right]^{-1}\cdot\overline{\overline{H}}_{01}\cdot\overline{\overline{F}}_{1-}(a_0)\right. \\ &\quad\left.-\left[\overline{\overline{F}}'_{0+}(a_0)+\overline{\overline{F}}'_{0-}(a_0)\cdot\tilde{\overline{\overline{R}}}_{\cup 0}\right]^{-1}\cdot\overline{\overline{H}}_{10}^t\cdot\overline{\overline{F}}'_{1-}(a_0)\right\}^{-1} \\ &\cdot\left\{\left[\overline{\overline{F}}'_{0+}(a_0)+\overline{\overline{F}}'_{0-}(a_0)\cdot\tilde{\overline{\overline{R}}}_{\cup 0}\right]^{-1}\cdot\overline{\overline{H}}_{10}^t\cdot\overline{\overline{F}}'_{1+}(a_0)\right. \\ &\quad\left.-\left[\overline{\overline{F}}_{0+}(a_0)+\overline{\overline{F}}_{0-}(a_0)\cdot\tilde{\overline{\overline{R}}}_{\cup 0}\right]^{-1}\cdot\overline{\overline{H}}_{01}\cdot\overline{\overline{F}}_{1+}(a_0)\right\} \\ &\cdot\overline{\overline{F}}_{1+}^{-1}(a_0). \end{aligned} \tag{18}$$

At $\rho = a_\ell$ with $\ell = 1, 2, \ldots, m-1$, impose the continuity conditions that $\Psi_\ell(a_\ell,\phi) = \Psi_{\ell+1}(a_\ell,\phi)$ and $\epsilon_\ell(\phi)\partial\Psi_\ell(a_\ell,\phi)/\partial\rho = \epsilon_{\ell+1}(\phi)\partial\Psi_{\ell+1}(a_\ell,\phi)/\partial\rho$ to have

$$\begin{aligned}&\left[\overline{\overline{F}}_{\ell+}(a_\ell)+\overline{\overline{F}}_{\ell-}(a_\ell)\cdot\overline{\overline{F}}_{\ell-}^{-1}(a_{\ell-1})\cdot\overline{\overline{R}}_{\cup\ell}\cdot\overline{\overline{F}}_{\ell+}(a_{\ell-1})\right]\cdot\overline{a}_\ell \\ &=\overline{\overline{H}}_{\ell(\ell+1)}\cdot\left[\overline{\overline{F}}_{(\ell+1)+}(a_\ell)+\overline{\overline{F}}_{(\ell+1)-}(a_\ell)\cdot\overline{\overline{F}}_{(\ell+1)-}^{-1}(a_\ell)\cdot\overline{\overline{R}}_{\cup(\ell+1)}\cdot\overline{\overline{F}}_{(\ell+1)+}(a_\ell)\right]\cdot\overline{a}_{(\ell+1)} \\ &\left[\overline{\overline{F}}'_{\ell+}(a_\ell)+\overline{\overline{F}}'_{\ell-}(a_\ell)\cdot\overline{\overline{F}}_{\ell-}^{-1}(a_{\ell-1})\cdot\overline{\overline{R}}_{\cup\ell}\cdot\overline{\overline{F}}_{\ell+}(a_{\ell-1})\right]\cdot\overline{a}_\ell \\ &=\overline{\overline{H}}_{(\ell+1)\ell}^t\cdot\left[\overline{\overline{F}}'_{(\ell+1)+}(a_\ell)+\overline{\overline{F}}'_{(\ell+1)-}(a_\ell)\cdot\overline{\overline{F}}_{(\ell+1)-}^{-1}(a_\ell)\cdot\overline{\overline{R}}_{\cup(\ell+1)}\cdot\overline{\overline{F}}_{(\ell+1)+}(a_\ell)\right]\cdot\overline{a}_{\ell+1}. \end{aligned} \tag{19}$$

A recursive formula for the potential ratio coefficient matrices is derived as

$$\begin{aligned}&\overline{\overline{R}}_{\cup(\ell+1)} \\ &=\left\{\left[\overline{\overline{F}}_{\ell+}(a_\ell)+\overline{\overline{F}}_{\ell-}(a_\ell)\cdot\overline{\overline{F}}_{\ell-}^{-1}(a_{\ell-1})\cdot\overline{\overline{R}}_{\cup\ell}\cdot\overline{\overline{F}}_{\ell+}(a_{\ell-1})\right]^{-1}\cdot\overline{\overline{H}}_{\ell(\ell+1)}-\left[\overline{\overline{F}}'_{\ell+}(a_\ell)+\overline{\overline{F}}'_{\ell-}(a_\ell)\cdot\overline{\overline{F}}_{\ell-}^{-1}(a_{\ell-1})\cdot\overline{\overline{R}}_{\cup\ell}\cdot\overline{\overline{F}}_{\ell+}(a_{\ell-1})\right]^{-1}\right. \\ &\quad\left.\cdot\overline{\overline{H}}_{(\ell+1)\ell}^t\cdot\overline{\overline{F}}'_{(\ell+1)-}(a_\ell)\cdot\overline{\overline{F}}_{(\ell+1)-}^{-1}(a_\ell)\right\}^{-1} \\ &\cdot\left\{\left[\overline{\overline{F}}'_{\ell+}(a_\ell)+\overline{\overline{F}}'_{\ell-}(a_\ell)\cdot\overline{\overline{F}}_{\ell-}^{-1}(a_{\ell-1})\cdot\overline{\overline{R}}_{\cup\ell}\cdot\overline{\overline{F}}_{\ell+}(a_{\ell-1})\right]^{-1}\right. \\ &\quad\cdot\overline{\overline{H}}_{(\ell+1)\ell}^t\cdot\overline{\overline{F}}'_{(\ell+1)+}(a_\ell)-\left[\overline{\overline{F}}_{\ell+}(a_\ell)+\overline{\overline{F}}_{\ell-}(a_\ell)\cdot\overline{\overline{F}}_{\ell-}^{-1}(a_{\ell-1})\cdot\overline{\overline{R}}_{\cup\ell}\cdot\overline{\overline{F}}_{\ell+}(a_{\ell-1})\right]^{-1} \\ &\quad\left.\cdot\overline{\overline{H}}_{\ell(\ell+1)}\cdot\overline{\overline{F}}_{(\ell+1)+}(a_\ell)\right\}\cdot\overline{\overline{F}}_{(\ell+1)+}^{-1}(a_\ell). \end{aligned} \tag{20}$$

Similarly, imposing the continuity conditions at $\rho = a_\ell$ that $\Psi_\ell(a_\ell, \phi) = \Psi_{\ell+1}(a_\ell, \phi)$ and $\epsilon_\ell(\phi)\partial\Psi_\ell(a_\ell, \phi)/\partial\rho = \epsilon_{\ell+1}(\phi)\partial\Psi_{\ell+1}(a_\ell, \phi)/\partial\rho$ with $\ell = m+1, m+2, \ldots, n-1$, we have

$$\begin{aligned}
&\overline{\overline{H}}_{(\ell+1)\ell} \\
&\quad \cdot \left[\overline{\overline{F}}_{\ell+}(a_\ell) \cdot \overline{\overline{F}}^{-1}_{\ell+}(a_\ell) \cdot \overline{\overline{R}}_{\cap\ell} \cdot \overline{\overline{F}}_{\ell-}(a_\ell) + \overline{\overline{F}}_{\ell-}(a_\ell)\right] \cdot \overline{b}_\ell \\
&= \Big[\overline{\overline{F}}_{(\ell+1)+}(a_\ell) \cdot \overline{\overline{F}}^{-1}_{(\ell+1)+}(a_{\ell+1}) \cdot \overline{\overline{R}}_{\cap(\ell+1)} \cdot \overline{\overline{F}}_{(\ell+1)-}(a_{\ell+1}) \\
&\qquad + \overline{\overline{F}}_{(\ell+1)-}(a_\ell)\Big] \cdot \overline{b}_{(\ell+1)} \\
&\overline{\overline{H}}^{\,t}_{\ell(\ell+1)} \\
&\quad \cdot \left[\overline{\overline{F}}'_{\ell+}(a_\ell) \cdot \overline{\overline{F}}^{-1}_{\ell+}(a_\ell) \cdot \overline{\overline{R}}_{\cap\ell} \cdot \overline{\overline{F}}_{\ell-}(a_\ell) + \overline{\overline{F}}'_{\ell-}(a_\ell)\right] \cdot \overline{b}_\ell \\
&= \Big[\overline{\overline{F}}'_{(\ell+1)+}(a_\ell) \cdot \overline{\overline{F}}^{-1}_{(\ell+1)+}(a_{\ell+1}) \cdot \overline{\overline{R}}_{\cap(\ell+1)} \cdot \overline{\overline{F}}_{(\ell+1)-}(a_{\ell+1}) \\
&\qquad + \overline{\overline{F}}'_{(\ell+1)-}(a_\ell)\Big] \cdot \overline{b}_{\ell+1}. \qquad (21)
\end{aligned}$$

Hence, another recursive formula is derived as

$$\begin{aligned}
&\overline{\overline{R}}_{\cap\ell} \\
&= \Big\{\Big[\overline{\overline{F}}_{(\ell+1)+}(a_\ell) \cdot \overline{\overline{F}}^{-1}_{(\ell+1)+}(a_{\ell+1}) \cdot \overline{\overline{R}}_{\cap(\ell+1)} \cdot \overline{\overline{F}}_{(\ell+1)-}(a_{\ell+1}) \\
&\qquad + \overline{\overline{F}}_{(\ell+1)-}(a_\ell)\Big]^{-1} \cdot \overline{\overline{H}}_{(\ell+1)\ell} \\
&\qquad - \Big[\overline{\overline{F}}'_{(\ell+1)+}(a_\ell) \cdot \overline{\overline{F}}^{-1}_{(\ell+1)+}(a_{\ell+1}) \cdot \overline{\overline{R}}_{\cap(\ell+1)} \\
&\qquad\quad \cdot \overline{\overline{F}}_{(\ell+1)-}(a_{\ell+1}) + \overline{\overline{F}}'_{(\ell+1)-}(a_\ell)\Big]^{-1} \\
&\qquad\quad \cdot \overline{\overline{H}}^{\,t}_{\ell(\ell+1)} \cdot \overline{\overline{F}}'_{\ell+}(a_\ell) \cdot \overline{\overline{F}}^{-1}_{\ell+}(a_\ell)\Big\}^{-1} \\
&\quad \cdot \Big\{\Big[\overline{\overline{F}}'_{(\ell+1)+}(a_\ell) \cdot \overline{\overline{F}}^{-1}_{(\ell+1)+}(a_{\ell+1}) \cdot \overline{\overline{R}}_{\cap(\ell+1)} \\
&\qquad \cdot \overline{\overline{F}}_{(\ell+1)-}(a_{\ell+1}) + \overline{\overline{F}}'_{(\ell+1)-}(a_\ell)\Big]^{-1} \cdot \overline{\overline{H}}^{\,t}_{\ell(\ell+1)} \\
&\qquad \cdot \overline{\overline{F}}'_{\ell-}(a_\ell) - \Big[\overline{\overline{F}}_{(\ell+1)+}(a_\ell) \cdot \overline{\overline{F}}^{-1}_{(\ell+1)+}(a_{\ell+1}) \\
&\qquad\qquad \cdot \overline{\overline{R}}_{\cap(\ell+1)} \cdot \overline{\overline{F}}_{(\ell+1)-}(a_{\ell+1}) \\
&\qquad\qquad + \overline{\overline{F}}_{(\ell+1)-}(a_\ell)\Big]^{-1} \cdot \overline{\overline{H}}_{(\ell+1)\ell} \cdot \overline{\overline{F}}_{\ell-}(a_\ell)\Big\} \\
&\quad \cdot \overline{\overline{F}}^{-1}_{\ell-}(a_\ell). \qquad (22)
\end{aligned}$$

Next, at the interface $\rho = a_m$ where the microstrip is located, impose the conditions that the potential distributions are continuous, and the discontinuity of normal electric flux density accounts for the charge distribution on the microstrip, namely,

$$\begin{aligned}
\Psi_m(a_m, \phi) &= \Psi_{m+1}(a_m, \phi) \\
\zeta(\phi) &= -\epsilon_m(\phi) \frac{\partial \Psi_m(a_m, \phi)}{\partial \rho} \\
&\quad + \epsilon_{m+1}(\phi) \frac{\partial \Psi_{m+1}(a_m, \phi)}{\partial \rho}. \qquad (23)
\end{aligned}$$

Applying the same technique as in deriving the recursive formulas of the potential ratio coefficient matrices, we obtain

$$\begin{aligned}
\overline{b}_{m+1} &= \overline{\overline{S}}_1 \cdot \overline{a}_m \\
\overline{\zeta}_m &= \overline{\overline{S}}_2 \cdot \overline{a}_m \qquad (24)
\end{aligned}$$

where

$$\begin{aligned}
\overline{\overline{S}}_1 &= \Big[\overline{\overline{F}}_{(m+1)+}(a_m) \cdot \overline{\overline{F}}^{-1}_{(m+1)+}(a_{m+1}) \cdot \overline{\overline{R}}_{\cap(m+1)} \\
&\qquad \cdot \overline{\overline{F}}_{(m+1)-}(a_{m+1}) + \overline{\overline{F}}_{(m+1)-}(a_m)\Big]^{-1} \cdot \overline{\overline{H}}_{(m+1)m} \\
&\quad \cdot \Big[\overline{\overline{F}}_{m+}(a_m) + \overline{\overline{F}}_{m-}(a_m) \cdot \overline{\overline{F}}^{-1}_{m-}(a_{m-1}) \cdot \overline{\overline{R}}_{\cup m} \\
&\qquad \cdot \overline{\overline{F}}_{m+}(a_{m-1})\Big] \\
\overline{\overline{S}}_2 &= \Big\{-\Big[\overline{\overline{F}}'_{m+}(a_m) + \overline{\overline{F}}'_{m-}(a_m) \cdot \overline{\overline{F}}^{-1}_{m-}(a_{m-1}) \\
&\qquad \cdot \overline{\overline{R}}_{\cup m} \cdot \overline{\overline{F}}_{m+}(a_{m-1})\Big] + \overline{\overline{H}}^{\,t}_{(m+1)m} \\
&\quad \cdot \Big[\overline{\overline{F}}'_{(m+1)+}(a_m) \cdot \overline{\overline{F}}^{-1}_{(m+1)+}(a_{m+1}) \cdot \overline{\overline{R}}_{\cap(m+1)} \\
&\qquad \cdot \overline{\overline{F}}_{(m+1)-}(a_{m+1}) + \overline{\overline{F}}'_{(m+1)-}(a_m)\Big] \cdot \overline{\overline{S}}_1\Big\} \\
\overline{\zeta}_m &= \langle \overline{\eta}_m(\phi), \zeta(\phi) \rangle. \qquad (25)
\end{aligned}$$

The coefficient $\overline{a}_m$ is thus expressed in terms of the charge coefficients $\overline{\zeta}_m$ as $\overline{a}_m = \overline{\overline{S}}^{-1}_2 \cdot \overline{\zeta}_m$

Finally, impose the boundary condition that the potential on the mircostrip surface is equal to the impressed voltage V_0 to form an integral equation with the charge distribution as unknown

$$\overline{\eta}^t_m(\phi) \cdot \overline{\overline{G}}_m \cdot \overline{\zeta}_m = V_0, \text{ on strip} \qquad (26)$$

where

$$\begin{aligned}
\overline{\overline{G}}_m &= \Big[\overline{\overline{F}}_{m+}(a_m) + \overline{\overline{F}}_{m-}(a_m) \cdot \overline{\overline{F}}^{-1}_{m-}(a_{m-1}) \cdot \overline{\overline{R}}_{\cup m} \\
&\qquad \cdot \overline{\overline{F}}_{m+}(a_{m-1})\Big] \cdot \overline{\overline{S}}^{-1}_2 \qquad (27)
\end{aligned}$$

can be viewed as the Green's function between the charge distribution and the potential.

To solve the integral equation, first choose a set of basis functions to expand the surface charge as

$$\zeta(\phi) = \sum_{s=0}^{N-1} \alpha_s f_s(\phi). \qquad (28)$$

The charge coefficients can then be expressed in terms of the coefficients $\{\alpha_s\}$ as

$$\overline{\zeta}_m = \sum_{s=0}^{N-1} \alpha_s \overline{f}_{sm} \qquad (29)$$

where $\overline{f}_{sm} = \langle \overline{\eta}_m(\phi), f_s(\phi) \rangle$. Substitute (29) into the integral equation, choose the same set of basis functions as weighting functions, and take the inner product of each weighting function with the resulting equation to obtain a matrix equation as

$$\langle V_0, f_r(\phi) \rangle = \sum_{s=0}^{N-1} \overline{f}^{\,t}_{rm} \cdot \overline{\overline{G}}_m \cdot \overline{f}_{sm} \alpha_s, \qquad 0 \le r < N. \qquad (30)$$

The per-unit-length capacitance is defined as the total per-unit-length charge over the impressed voltage, which is obtained by integrating the surface charge density over the microstrip surface in the ϕ-direction. The characteristic impedance of the transmission line is calculated as

$$Z_c = \frac{1}{v_0\sqrt{C\,C_0}} \tag{31}$$

where v_0 is the velocity of light in free space, C_0 is the per-unit-length capacitance in free space, and C is the per-unit-length capacitance of the transmission line.

III. Results and Discussions

A convergence test has been presented in [21] on the characteristic impedance of a stripline inserted in a coaxial cable with respect to mode and basis numbers. It is shown that the numerical results converge as the mode number is greater than 60. It is also found that more modes are needed to obtain convergent results when the basis number is increased. Using more modes implies better resolution for the charge distribution, but longer CPU time. It takes a few seconds to obtain one characteristic impedance with 100 modes, using a personal computer with a Pentium III CPU 600-MHz clock rate. The CPU time can be further reduced if tabulation technique is used to store repeatedly used data.

Fig. 2 shows the impedance of coupled cylindrical striplines as a function of strip separation and mode number for both the even and odd modes. Our results match well with those in [7]. Coupling effects between conductors can be described by equivalent capacitors. Since the two metal strips are surrounded by two grounded cylinders, capacitance between each metal strip and each grounded cylinder exists for both the even and odd modes. An extra field coupling exists between the two metal strips for the odd mode, which is associated with an extra coupling capacitor. Thus, the capacitance of the odd mode is higher than that of the even mode; hence, the characteristic impedance of the odd mode is less than that of the even mode. As the strips are separated farther apart, the coupling effects between them become less obvious, and the deviation of characteristic impedance reduces.

Fig. 3 shows the variation of characteristic impedance of a single stripline with the span angle α of the strip. Since the capacitance is roughly proportional to the strip span angle, the characteristic impedance is almost inversely proportional to the span angle α. This implies that impedance matching with other circuits can be achieved by adjusting the width of a cylindrical stripline in addition to the radius or the dielectric constant of the layered medium [13].

Fig. 4 shows the effective dielectric constant of a stripline on top of an inhomogeneous layer that encloses a homogeneous layer with relative dielectric constant ϵ_r. A region with a relatively higher dielectric constant tends to induce stronger electric field. Hence, the effective dielectric constant increases as ϵ_r increases. The variation of electric-field distribution can be explained by viewing the structure as three equivalent capacitors. The first one is between the metal strip and outer cylinder, the second one is between the metal strip and interface at $\rho = a_1$, and the third one is between the inner cylinder and the interface

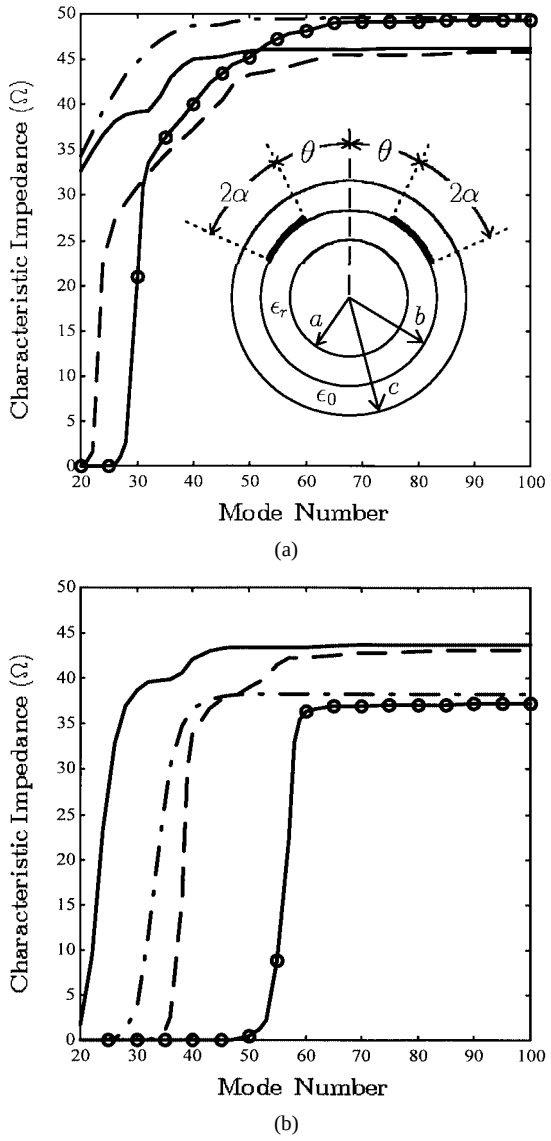

Fig. 2. Effect of mode number on the characteristic impedance of two coupled striplines, $b/a = 1.4$, $c/a = 1.8$, $\epsilon_r = 2.55$, $\alpha = 20°$. —: $\theta = 10°$, ten bases. – –: $\theta = 10°$, 16 bases. -·-: $\theta = 2°$, ten bases. -o- $\theta = 2°$, 16 bases. (a) Even mode. (b) Odd mode. The characteristic impedance of the even mode in [7] is 45.02 Ω for $\theta = 10°$, 48.77 Ω for $\theta = 2°$, and that of the odd mode is 42.23 Ω for $\theta = 10°$, 35.45 Ω for $\theta = 2°$.

at $\rho = a_1$. The first capacitor is in shunt with the series combination of the second and third ones. The series capacitance of the second and third capacitors increases as ϵ_r increases, and the first capacitor is invariant to ϵ_r, Thus, the effective dielectric constant increases with increasing ϵ_r. Due to the wide free space above the strip, the effective dielectric constant increases less slowly than ϵ_r does. Hence, the range of effective dielectric constant is smaller than that of ϵ_r. It is observed that the effective dielectric constant is almost independent of the strip width, and appears almost as a linear function of the substrate dielectric constant, similar to those in [18].

Fig. 5 shows the effective dielectric constant of a stripline supported by a thin membrane. An air pocket is created beneath the strip to increase the phase velocity of the line. The variation of electric-field distribution can be understood by using four equivalent capacitors. The first one is between the metal strip

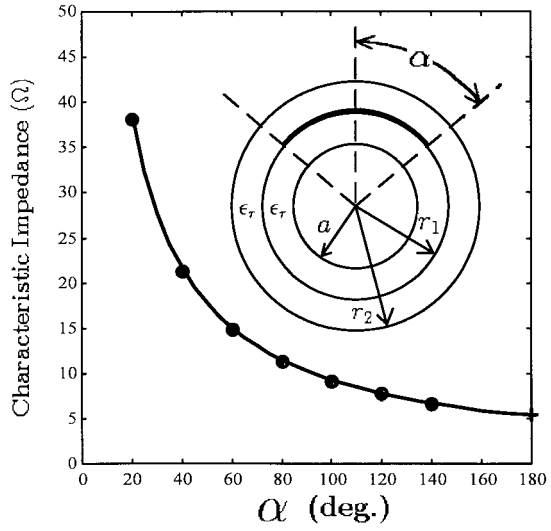

Fig. 3. Variation of characteristic impedance with α, $r_1/a = 1.8$, $r_2/a = 2.0$, $\epsilon_r = 1.0$. —: this approach. ∘: results in [6]. +: results in [7].

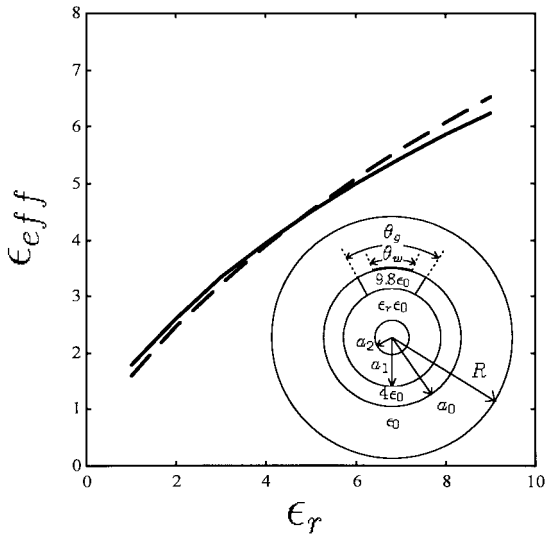

Fig. 4. Effect of underlying layer ϵ_r on the effective dielectric constant of a stripline on a segmented inhomogeneous substrate $a_0/R = 0.6$, $a_1/R = 17/30$, $a_2/R = 0.5$, $\theta_g = 80°$. —: $\theta_w = 20°$. – –: $\theta_w = 40°$.

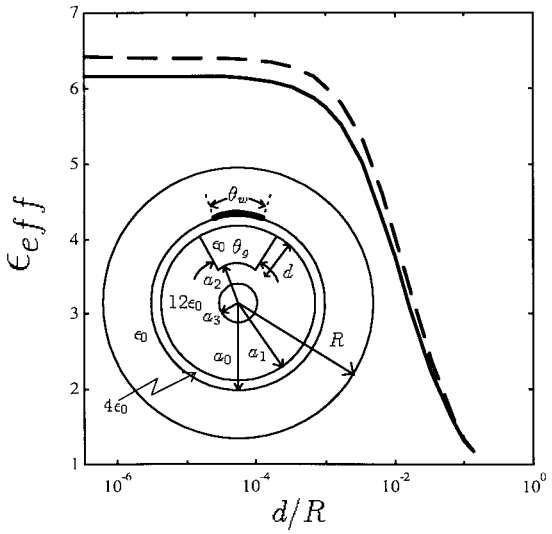

Fig. 5. Effect of air-pocket depth on the effective dielectric constant of a stripline supported by a thin membrane $a_0/R = 20.2/30$, $a_1/R = 2/3$, $a_2/R = 0.5$, $\theta_g = 80°$. —: $\theta_w = 20°$. – –: $\theta_w = 40°$.

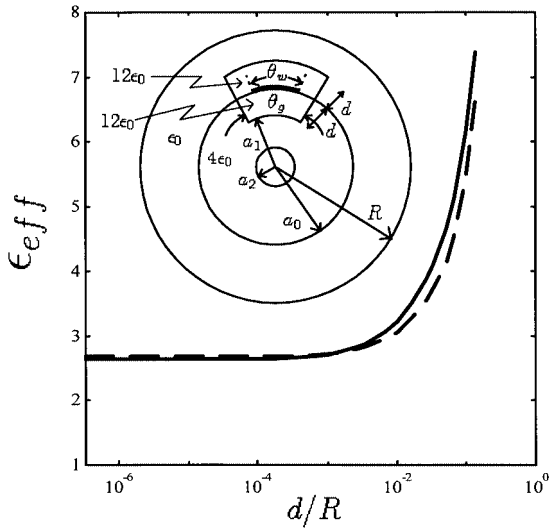

Fig. 6. Effect of enclosure depth on the effective dielectric constant of a stripline enclosed by a region with high dielectric constant $a_0/R = 2/3$, $a_2/R = 0.5$, $\theta_g = 80°$. —: $\theta_w = 20°$, – –: $\theta_w = 40°$.

and outer cylinder, the second one is between the metal strip and the interface at $\rho = a_1$, the third one is between the interfaces at $\rho = a_1$ and $\rho = a_2$, and the fourth one is between the interface at $\rho = a_2$ and the inner cylinder. The first capacitor is in shunt with the series combination of the second, the third, and the fourth ones. The third capacitance decreases and the fourth capacitance increases as d increases. Since the substrate has a much higher permittivity than free space, the series capacitance of the third and fourth capacitors decreases as d increases. The first and second capacitors are invariant to the depth d. Hence, the effective dielectric constant decreases with the air-pocket depth. It is confirmed that the air pocket increases the phase velocity of the line and the effects become obvious when the pocket is deeper than $0.001R$. It is also found that a wider strip tends to incur a slower phase velocity.

Fig. 6 shows the effective dielectric constant of a stripline enclosed by a region with high dielectric constant to reduce its phase velocity. Four equivalent capacitors can be used to describe the variation of electric-field distribution. The first one is between the top of the enclosure region and the outer cylinder, the second one is between the metal strip and the top of the enclosure region, the third one is between the metal strip and the bottom of the enclosure region, and the fourth one is between the bottom of the enclosure region and the inner cylinder. The series combination of the first and second ones are in shunt with the series combination of the third and fourth ones. The extent of high-permittivity enclosure increases with d. As d increases, the first and fourth capacitances increase, but the second and third ones decrease. Since the enclosure region has a much higher permittivity than free space and the substrate, the series capacitance of the first and second ones increases, and the series capacitance of the third and fourth ones increases as d increases. The total capacitance increases with the enclosure depth and so does the

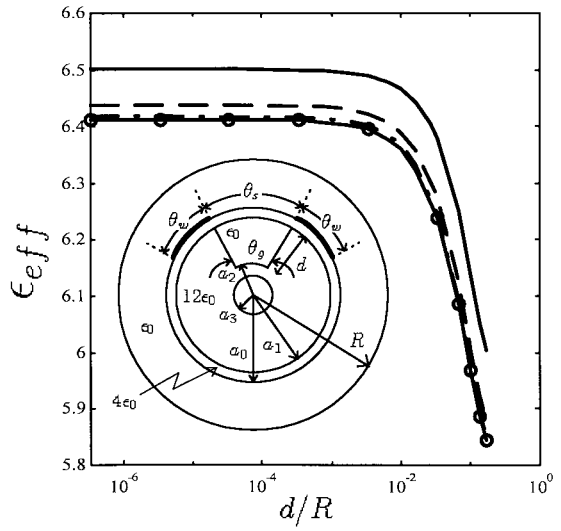

(a)

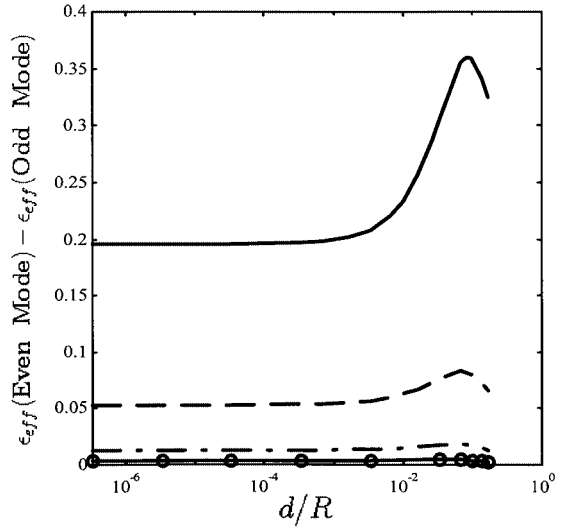

(b)

Fig. 7. Effect of air pocket depth on the effective dielectric constant of the even mode for two coupled striplines $a_0/R = 20.2/30$, $a_1/R = 2/3$, $a_2/R = 0.5$, $\theta_w = 40°$. —: $\theta_g = 20°$, – –: $\theta_g = 40°$. -·-: $\theta_g = 60°$. -o-: $\theta_g = 80°$. (a) Even mode. (b) Deviation between even and odd modes.

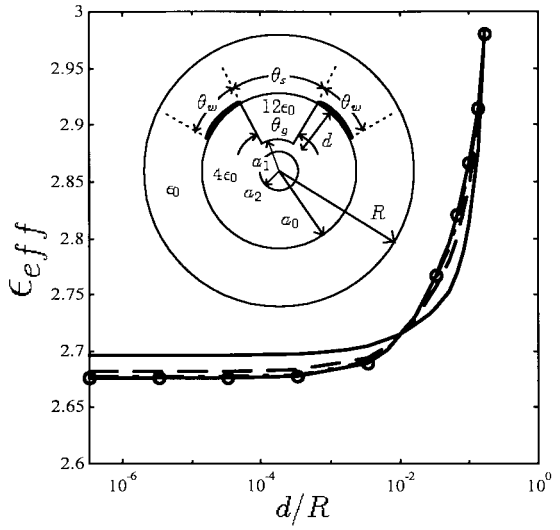

(a)

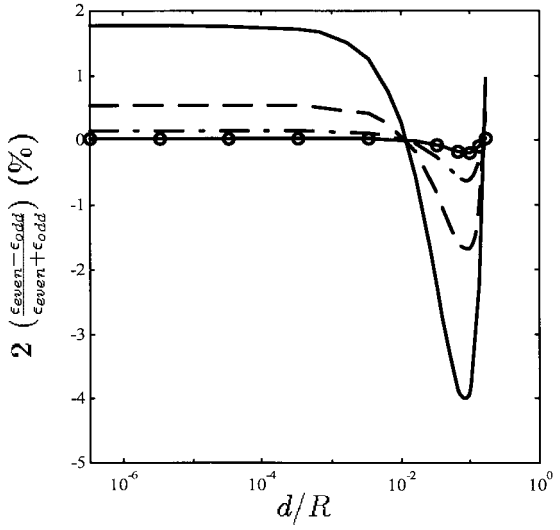

(b)

Fig. 8. Effect of channel thickness on the effective dielectric constant of the even mode for two coupled striplines $a_0/R = 2/3$, $a_2/R = 0.5$, $\theta_w = 40°$. —: $\theta_g = 20°$, – –: $\theta_g = 40°$. -·-: $\theta_g = 60°$. -o-: $\theta_g = 80°$. (a) Even mode. (b) Deviation between even and odd modes.

effective dielectric constant. It is observed that the enclosure region begins to have an obvious effect as the enclosure thickness is greater than $0.001R$. The effect is more obvious for a narrower strip. For a wider strip, more electric field tends to pass through the region outside of the enclosure. Thus, the effective dielectric constant is relatively smaller.

Fig. 7 shows the effective dielectric constant of the even mode for two coupled striplines supported by a thin membrane. The air pocket below the thin membrane is intended to increase the phase velocity of the guided mode. In Fig. 7(a), the air pocket extends between the inner edges of the two coupled striplines. It is observed that the effects become obvious when the pocket is deeper than $0.01R$. The effective dielectric constant decreases as the two striplines are moved apart. More electric fields pass through the air pocket when its depth increases. Thus, the effective dielectric constant is reduced. Fig. 7(b) shows the deviation between the even and odd modes of two coupled striplines. The deviation first increases then decreases as the depth of the air pocket increases. It is expected that when the two lines are far apart, the mode dispersion between the two lines becomes smaller, and the effective dielectric constant of either mode approaches that of a single line. By this argument, the results imply that the mode dispersion is strongest where the pocket depth is around $0.1R$.

Fig. 8(a) shows the effective dielectric constant of the even mode for two coupled striplines with a block of high dielectric constant inserted in the substrate between the two lines. The high dielectric-constant region tends to focus more electric fields, thus the effective dielectric constant increases as the depth of the high permittivity region increases. The increase of effective dielectric constant is more obvious as the thickness

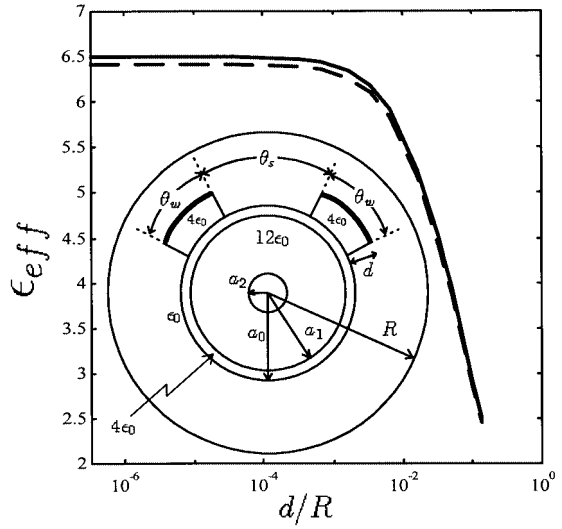

(a)

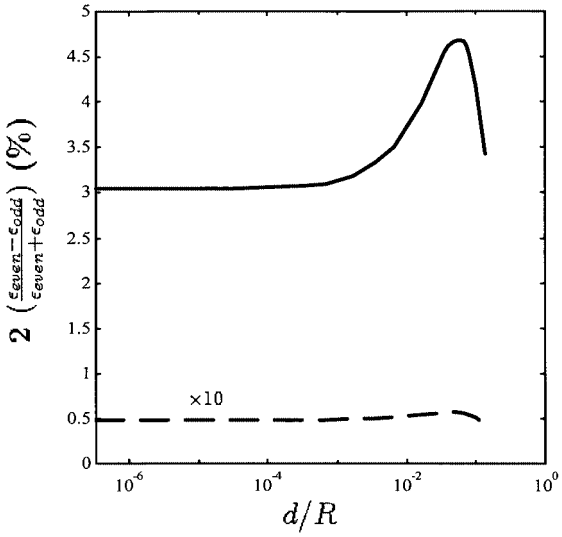

(b)

Fig. 9. Effect of buffer thickness on the effective dielectric constant of the even and odd modes for two coupled striplines $a_0/R = 2/3$, $a_2/R = 0.5$, $\theta_w = 40°$. —: $\theta_s = 20°$. – –: $\theta_s = 80°$. (a) Even mode. (b) Deviation between even and odd modes.

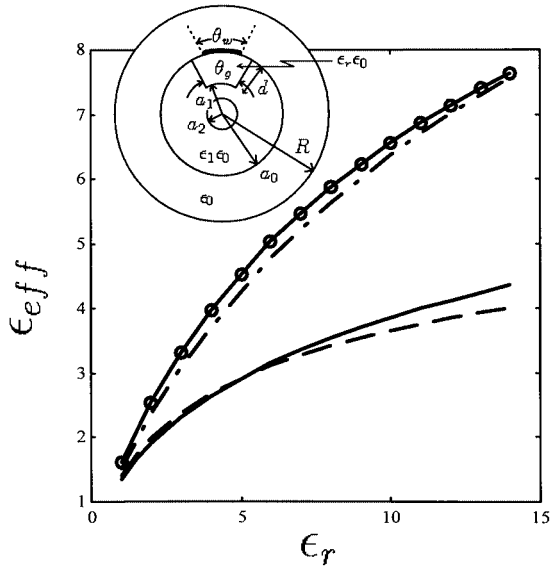

Fig. 10. Effect of small region ϵ_r on the effective dielectric constant of a stripline above a small region with ϵ_r, $a_0/R = 2/3$, $a_1/R = 0.6$, $a_2/R = 0.5$, $\theta_g = 40°$. —: $\epsilon_1 = 4$ and $\theta_w = 20°$. – –: $\epsilon_1 = 4$ and $\theta_w = 40°$. -·-: $\epsilon_1 = 12$ and $\theta_w = 20°$. -o-: $\epsilon_1 = 12$ and $\theta_w = 40°$.

of the region increases. For the odd modes, the inserted region becomes a channel that guides the electric fields between the two coupled striplines. More electric fields are confined by this channel when the region becomes thicker, thus the effective dielectric constant increases.

Fig. 8(b) shows the deviation between the even and odd modes for the same structure. The deviation vanishes when the depth of the high-permittivity region is varied from $0.001R$ to $0.01R$. This implies that the mode dispersion of this structure can be adjusted to zero. The deviation turns negative when the depth of the high-permittivity region is increased from $0.1R$. As the channel becomes thicker, more electric fields are confined between the two striplines through the channel. Thus, the effective dielectric constant of the odd mode increases more obviously than that of the even mode. As the bottom of the channel moves closer to the inner conductor, more electric fields tend to be attracted to the inner conductor. Thus, the dielectric constant of the even mode increases more obviously with increasing depth of the high-permittivity region than that of the odd mode.

Fig. 9(a) shows the effective dielectric constant of the even mode for two coupled striplines supported by isolated buffers having a lower dielectric constant than the host substrate. As the buffers become thicker, the electric field emerging from the strip surface passes through a wider area with lower dielectric constant than the host substrate. Thus, the effective dielectric constant decreases. It is also observed that the buffers begin to have an obvious effect as their thickness is greater than $0.001R$. Fig. 9(b) shows the percentage deviation of effective dielectric constant between the even and odd modes. As the buffers become thicker, the deviation first increases, and then decreases. Also notice that, as the separation between the two strips increases, the percentage deviation between the even and odd modes decreases. The deviation for the case of $\theta_s = 80°$ in Fig. 9(b) is magnified by tenfold to make it more readable.

Fig. 10 shows the effective dielectric constant of a stripline on top of an inserted buffer with relative dielectric constant ϵ_r. The inserted buffer tends to concentrate more electric fields as ϵ_r increases. Thus, the effective dielectric constant increases as the relative dielectric constant ϵ_r increases. The range of effective dielectric constant is smaller than that of ϵ_r since part of the electric fields pass through free space. Also notice that the range of the effective dielectric constant is wider when the dielectric constant of the host substrate is higher.

Fig. 11(a) shows the effective dielectric constant of the even mode for two coupled striplines with an inserted buffer permittivity. The results are similar to those of a single stripline, as shown in Fig. 10. Fig. 11(b) shows the deviation between the two modes. The deviation between the two modes with $\epsilon_1 = 4$

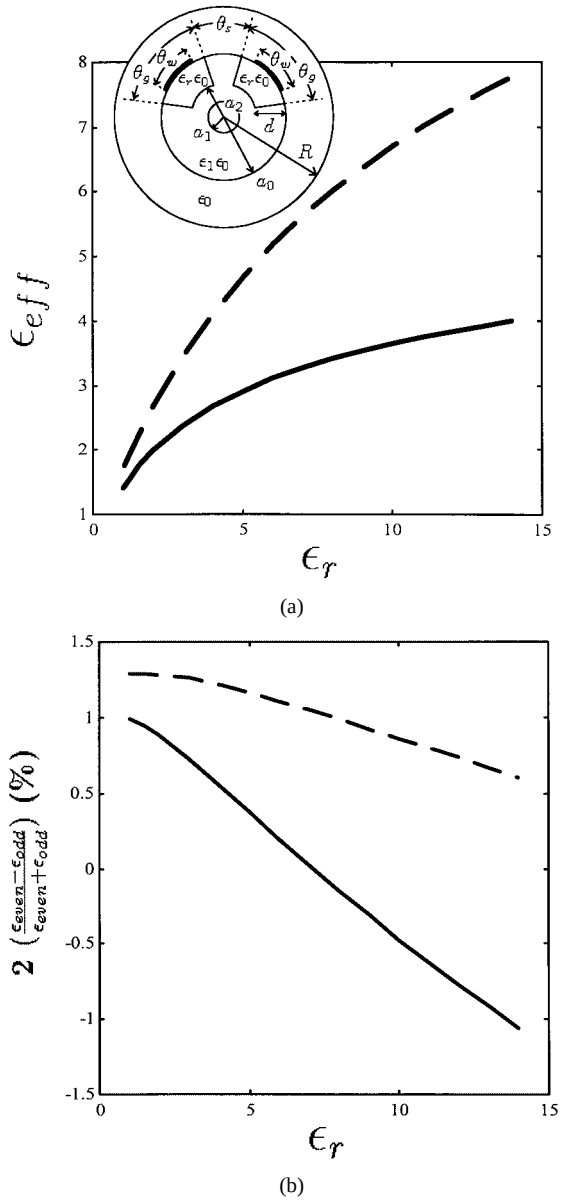

Fig. 11. Effect of small-region ϵ_r on the effective dielectric constant of the even and odd modes for two coupled striplines $a_0/R = 2/3$, $a_1/R = 0.6$, $a_2/R = 0.5$, $\theta_w = 40°$, $\theta_g = 60°$, $\theta_s = 20°$. —: $\epsilon_1 = 4$. – –: $\epsilon_1 = 12$. (a) Even mode. (b) Deviation between even and odd modes.

reduces to zero when ϵ_r is near seven, which implies that the mode dispersion vanishes.

IV. Conclusions

A mode-matching technique combined with Galerkin's method is proposed in this paper to study the characteristics of striplines embedded in a cylindrically layered medium inhomogeneous in the azimuthal direction, which has not been studied before. A convergence test with respect to the mode number and basis number, as well as a comparison with the literature verify the effectiveness of this approach. Several inhomogeneous dielectric profiles are studied to understand the effects of inhomogeneities on the characteristic impedance, effective dielectric constant, and phase velocity of the striplines. Underneath a stripline, a local region with higher permittivity tends to focus the field distribution, and an air pocket tends to increase the phase speed of the guided signal. A combination of equivalent capacitors can be used to explain the variation of the field distribution. A high-permittivity enclosure, dielectric buffers, dielectric insertions, or air pocket can be used to control the coupling between two transmission lines. Proper adjustment of geometrical and electric parameters of these inhomogeneities will eliminate mode dispersion along coupled transmission lines, hence, a reduction of signal distortion along these lines.

References

[1] S. Xiao, R. Vahldieck, and J. Hesselbarth, "Analysis of cylindrical transmission lines with the method of lines," *IEEE Trans. Microwave Theory Tech.*, vol. 44, pp. 993–999, July 1996.

[2] M. A. Kolbehdari and M. S. Nakhla, "Electromagnetic modeling and simulation of multiconductor interconnect networks with inhomogeneous cylindrical substrate," *Proc. Inst. Elect. Eng.*, pt. H, vol. 144, pp. 347–353, Oct. 1997.

[3] L.-R. Zeng and Y. Wang, "Accurate solutions of elliptical and cylindrical striplines and microstrip lines," *IEEE Trans. Microwave Theory Tech.*, vol. MTT-34, pp. 259–265, Feb. 1986.

[4] D. Homentcovschi, G. Ghione, C. Naldi, and R. Oprea, "Analytic determination of the capacitance matrix of planar or cylindrical multiconductor lines on multilayered substrates," *IEEE Trans. Microwave Theory Tech.*, vol. 43, pp. 363–373, Feb. 1995.

[5] D. Homentcovschi, "A cylindrical multiconductor stripline-like microstrip transmission line," *IEEE Trans. Microwave Theory Tech.*, vol. 37, pp. 497–503, Mar. 1989.

[6] C. H. Chan and R. Mittra, "Analysis of a class of cylindrical multiconductor transmission lines using an iterative approach," *IEEE Trans. Microwave Theory Tech.*, vol. MTT-35, pp. 415–424, Apr. 1987.

[7] F. Medina and M. Horno, "Spectral and variational analysis of generalized cylindrical and elliptical strip and microstrip lines," *IEEE Trans. Microwave Theory Tech.*, vol. 38, pp. 1287–1293, Sept. 1990.

[8] K. Gu and Y. Wang, "Analysis of dispersion characteristics of cylindrical microstrip line with method of lines," *Electron. Lett.*, vol. 26, no. 11, pp. 748–750, May 1990.

[9] N. G. Alexópoulos and A. Nakatani, "Cylindrical substrate microstrip line characterization," *IEEE Trans. Microwave Theory Tech.*, vol. MTT-35, pp. 843–849, Sept. 1987.

[10] A. Nakatani and N. G. Alexópoulos, "Coupled microstrip lines on a cylindrical substrate," *IEEE Trans. Microwave Theory Tech.*, vol. MTT-35, pp. 1392–1398, Dec. 1987.

[11] K. K. Joshi and B. N. Das, "Analysis of elliptic and cylindrical striplines using Laplace's equation," *IEEE Trans. Microwave Theory Tech.*, vol. MTT-28, pp. 381–386, Apr. 1980.

[12] M. A. Kolbehdari and M. N. O. Sadiku, "Finite and infinite element analysis of coupled cylindrical microstrip line in a nonhomogeneous dielectric media," in *IEEE Southeast Conf.*, 1995, pp. 269–273.

[13] T. Kitamura, T. Koshimae, M. Hira, and S. Kurazono, "Analysis of cylindrical microstrip lines utilizing the finite difference time domain method," *IEEE Trans. Microwave Theory Tech.*, vol. 42, pp. 1279–1282, July 1994.

[14] N. Dib, T. Weller, M. Scardelletti, and M. Imparato, "Analysis of cylindrical transmission lines with the finite difference time domain method," *IEEE Trans. Microwave Theory Tech.*, vol. 47, pp. 509–512, July 1999.

[15] N. Dib, T. Weller, and M. Scardelletti, "Analysis of 3-D cylindrical structures using the finite difference time domain method," in *IEEE MTT-S Int. Microwave Symp. Dig.*, 1998, pp. 925–928.

[16] J. Zehentner and P. Zörnig, "Longitudinal current density on out- and in-side cylindrical microstrip lines," *IEEE Trans. Microwave Theory Tech.*, vol. 42, pp. 1100–1102, June 1994.

[17] C. J. Reddy and M. D. Deshpande, "Analysis of cylindrical stripline with multilayer dielectrics," *IEEE Trans. Microwave Theory Tech.*, vol. MTT-34, pp. 701–706, June 1986.

[18] H. A. Auda, "Cylindrical microstrip line partially embedded in a perfectly conducting ground plane," *IEEE Trans. Microwave Theory Tech.*, vol. 39, pp. 1662–1666, Sept. 1991.

[19] J.-F. Kiang, "Capacitance of microstrip lines with inhomogeneous substrate," *IEEE Trans. Microwave Theory Tech.*, vol. 44, pp. 1703–1709, Oct. 1996.

[20] J.-F. Kiang, C.-I. G. Hsu, and C.-H. Lee, "Wedge-supported cylindrical microstrip lines with an indented ground," *IEICE Trans. Electron.*, vol. E81-C, pp. 1358–1365, Aug. 1998.
[21] C.-R. Lee, J.-F. Kiang, and C. H. Chen, "Characteristics of striplines with inhomogeneous cylindrical substrate," in *Asia–Pacific Microwave Conf.*, Taipei, Taiwan, R.O.C., Dec. 3–6, 2001, pp. 177–180.

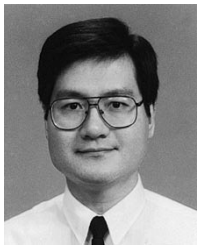

Jean-Fu Kiang (S'87–M'87) was born in Taipei, Taiwan, R.O.C., on February 2, 1957. He received the B.S. and M.S. degrees from the National Taiwan University, Taipei, Taiwan, R.O.C., in 1979 and 1981, respectively, and the Ph.D. degree from Massachusetts Institute of Technology, Cambridge, in 1989, all in electrical engineering.

From 1985 to 1986, he was with Schlumberger-Doll Research, Ridgefield, CT. From 1989 to 1990, he was with the IBM Watson Research Center, Yorktown Heights, NY. From 1990 to 1992, he was with Bellcore, Red Bank, NJ. From 1992 to 1994, he was with Siemens Electromedical Systems, Danvers, MA. From 1994 to 1999, he was with the National Chung-Hsing University, Taichung, Taiwan, R.O.C. Since 1999, he has been a Professor with the Department of Electrical Engineering and the Graduate Institute of Communication Engineering, National Taiwan University. His research interests are the applications and system issues on electromagnetics, including wireless communications, antennas, electromagnetic compatibility, microwave components, etc.

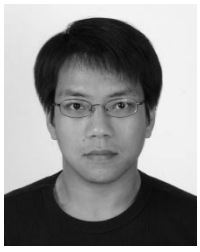

Chung-Rung Lee was born in Taipei, Taiwan, R.O.C., on July 23, 1976. He received the B.S. degree in communication engineering from the National Chiao-Tung University, Taiwan, R.O.C., in 1999, and the M.S. degree in communication engineering from the National Taiwan University, Taipei, Taiwan, R.O.C., in 2001.

In 2001, he joined the Department of Wireless Communication Production, MediaTek Inc., Taiwan, R.O.C., where he is currently an Application Engineer. His research interests are system application and testing of global system for mobile communications (GSM) and general packet radio service (GPRS) mobile phones.

Chun Hsiung Chen (SM'88–F'96) was born in Taipei, Taiwan, R.O.C., on March 7, 1937. He received the B.S.E.E. and Ph.D. degrees in electrical engineering from the National Taiwan University, Taipei, Taiwan, R.O.C., in 1960 and 1972, respectively, and the M.S.E.E. degree from the National Chiao Tung University, Hsinchu, Taiwan, R.O.C., in 1962.

In 1963, he joined the Faculty of the Department of Electrical Engineering, National Taiwan University, where he is currently a Professor. From August 1982 to July 1985, he was Chairman of the Department of Electrical Engineering at the same university. From August 1992 to July 1996, he was the Director of the University Computer Center. In 1974, he was a Visiting Scholar with the Department of Electrical Engineering and Computer Sciences, University of California at Berkeley. From August 1986 to July 1987, he was a Visiting Professor with the Department of Electrical Engineering, University of Houston, Texas. In 1989, 1990, and 1994, he visited the Microwave Department, Technical University of Munich, Munich, Germany, the Laboratoire d'Optique Electromagnetique, Faculte des Sciences et Techniques de Saint-Jerome, Universite d'Aix-Marseille III, Marseille, France, and the Department of Electrical Engineering, Michigan State University, East Lansing, respectively. His areas of interest include microwave circuit analysis and computational electromagnetics.